Antigen-Adjuvant Interactions in Vaccines by Taylor Dispersion Analysis: Size Characterization and Binding Parameters

Camille Malburet, Laurent Leclercq, Jean-François Cotte, Jérôme Thiebaud, Sergio Marco, Marie-Claire Nicolaï, Hervé Cottet

Antigen-adjuvant interactions in vaccines by Taylor dispersion analysis: size characterization and binding parameters

Camille Malburet[1,2], Laurent Leclercq[1], Jean-François Cotte[2], Jérôme Thiebaud[2], Sergio Marco[2], Marie-Claire Nicolaï[2], Hervé Cottet[1*]

1 IBMM, University of Montpellier, CNRS, ENSCM, Place Eugène Bataillon, 34095 Montpellier, France

2 Sanofi Pasteur, Analytical Sciences, 1541 avenue Marcel Mérieux, 69280 Marcy l'Etoile, France

* Corresponding author: herve.cottet@umontpellier.fr

ABSTRACT: Vaccine adjuvants are immunostimulatory substances used to improve and modulate the immune response induced by antigens. A better understanding of the antigen-adjuvant interactions is necessary to develop future effective vaccine. In this study, Taylor dispersion analysis (TDA) was successfully implemented to characterize the interactions between a polymeric adjuvant (poly(acrylic acid), SPA09) and a vaccine antigen in development for the treatment of *Staphylococcus aureus*. TDA allowed to rapidly determine both (*i*) the size of the antigen-adjuvant complexes under physiological conditions, and (*ii*) the percentage of free antigen in the adjuvant/antigen mixture at equilibrium, and finally get the interaction parameters (stoichiometry and binding constant). The complex sizes obtained by TDA were compared to the results obtained by transmission electron microscopy (TEM) and the binding parameters were compared to results previously obtained by frontal analysis continuous capillary electrophoresis (FACCE).

Used for over 100 years, vaccination remains one of the most impactive developments of modern medicine, allowing today to prevent several infections that once plagued humanity[1]. Yet, many infectious diseases are still lacking effective treatment and new diseases are emerging every year. Furthermore, vaccines have now the potential to not only prevent infectious diseases but also treat diseases such as cancer and neurodegenerative disorders[2–4].

Most vaccines in development are based on well-defined purified antigens. However, the immune response induced by these purified antigens alone is often insufficient[5,6]. The induction of an immune response of sufficient magnitude and duration may require the co-administration of an adjuvant. An adjuvant is an immunostimulatory substance used to modulate and enhance the immune response induced by an antigen[7]. Therefore, the development of new adjuvants goes hand in hand with the development of new vaccines. Choosing a suitable adjuvant to increase the immune response of a new antigen is often complex since knowledge about adjuvant activity is still limited[8]. Ideally, future vaccines should be developed with adjuvants of predictable activity. To reach that goal, the development of new analytical methods allowing to characterize antigen-adjuvant interactions is crucial to better understand the mode of action of the adjuvants and to improve the effectiveness of future vaccines.

Among other parameters, the size of the antigen-adjuvant complexes has been shown to have a significant impact on the immunity[9,10]. Some analytical techniques are already commonly used to study the size of proteins and their complexes with adjuvants: dynamic light scattering (DLS), size exclusion chromatography (SEC) coupled with multiple detections, analytical ultracentrifugation (AUC) and direct visualization techniques, such as transmission electron microscopy (TEM). However, all of these techniques have their own limitations, as the sensitivity to small quantities of larger molecules or dusts for DLS, the expensive cost of the instrumentation

for AUC or TEM, the undesirable interactions with stationary phase and abnormal elution profiles for SEC and the long duration of analysis.

Taylor dispersion analysis (TDA) has recently paid more and more attention and appears as a competitive and alternative technique for the determination of diffusion coefficients and hydrodynamic *radii* of proteins, macromolecules, nanoparticles, and their assemblies[11–17]. TDA is an absolute method based on the analysis of the dispersion of a solute plug in a capillary under a laminar Poiseuille flow, due to the combined action of convection and molecular diffusion. From the elution profile, it is possible to determine the molecular diffusion coefficient (D) and therefore the hydrodynamic radius (R_h) of solutes ranging from angstroms to submicrons[18,19]. In the case of mixtures composed of two populations of different sizes, which are both stable at the time scale of the analysis, TDA signal is the sum of two Gaussian peaks. The fitting of the elution profile allows to get the hydrodynamic radius of the two individual populations constituting the mixture and their relative proportions[20,21]. The access to the free ligand proportion allows to determine the isotherm of adsorption, and by curve fitting, the parameters of interaction (intrinsic binding constant and stoichiometry of interaction)[22]. TDA can also be used to study substrate/ligand interactions at equilibrium, when the two entities in interaction are in fast exchange at the time scale of the analysis. Due to fast kinetics of exchange, the taylorgram is a simple Gaussian peak which can be fitted to determine the binding constant by monitoring the change in diffusivity (or size) according to the ligand concentration introduced into the capillary[23–27].

Polymers including acrylic acid units have been used as vaccine adjuvant since the 1970s[28]. Since then, high molecular weight, crosslinked polyacrylic acid polymers are used as effective adjuvants in several veterinary vaccines[29,30] and are studied for the development of new human

vaccines[31,32]. SPA09 is a purified linear polyacrylic acid (PAA) polymer, which has been identified as a promising human adjuvant[33,34]. *Staphylococcus aureus* is the most frequently isolated bacterial pathogen from patients with hospital-acquired infections[35]. Treatment of *Staphylococcus aureus* infections is challenging as the strains are increasingly resistant to antibiotics. To counter antibiotic resistance new treatment strategies need to be developed with a focus on vaccine development[36,37]. After a method optimization using three model proteins (Cyt C, RNase A and BSA), TDA was successfully implemented to determine the size of the complexes and the interaction parameters between a polymeric adjuvant (SPA09) and a vaccine antigen in development for the treatment of *Staphylococcus aureus* (PrSA).

EXPERIMENTAL SECTION

Chemicals and Materials. SPA09[33] (PAA, M_w = 590 kDa, *PDI* = 2.2) at 17.8 g/L and PrSA (peptidyl-prolyl cis−trans isomerase from *S. aureus*, M_w = 35 kDa, *pI* = 9) at 1.6 g/L were provided by Sanofi Pasteur (Marcy-l'Étoile, France) in phosphate-buffered saline buffer (PBS). Cytochrome C from bovine heart (Cyt C, M_w = 12 kDa, *pI* = 10), ribonuclease A from bovine pancreas (RNase A, M_w = 14 kDa, *pI* = 9), bovine serum albumin (BSA, M_w = 66 kDa, *pI* = 5), TRIS ($(CH_2OH)_3CNH_2$, M_w = 121 g/mol), hydroxypropyl cellulose (HPC, $M_w = 1 \times 10^5$ g/mol), phosphoric acid (H_3PO_4, M_w = 98 g/mol) and monobasic sodium phosphate (NaH_2PO_4, M_w = 120 g/mol) were purchased from Merck (Darmstadt, Germany). Dimethylformamide (DMF, M_w = 73 g/mol) was purchased from Carlo Erba Reagents (Val-de-Reuil, France). Bare fused silica capillaries were purchased from Molex Polymicro Technologies (Phoenix, USA). Polyvinyl Alcohol (PVA) and Polyethylene glycol (DB-WAX) coated capillaries were purchased from Agilent Technologies (Santa Clara, USA). Deionized water was further purified with a Milli-Q system from Millipore (Molsheim, France). The SPA09 provided by Sanofi-Pasteur was dialyzed

against Milli-Q water in order to eliminate the PBS buffer using Slide-A-Lyzer Dialysis Cassette G2 3 500 M_wCO (ThermoFisher Scientific, Waltham, USA), and then freeze-dried. All the other chemicals were used without any further treatment.

Sample preparation. Stock solutions of Cyt C, RNase A and BSA were prepared at 3.2 g/L in TRIS buffer (20 mM TRIS, 148 mM NaCl) at pH 7.4. PrSA was provided at 1.6 g/L in PBS buffer (10 mM PBS, 150 mM NaCl) at pH 7.2. Two stock solutions of SPA09 at 2 g/L were prepared: one in TRIS buffer at pH 7.4 and one in PBS buffer at pH 7.2. All the stock solutions were subsequently diluted to the desired concentrations in TRIS or PBS buffer. The antigen-adjuvant mixtures (× 1) were obtained by mixing 150 µL of antigen solution and 150 µL of adjuvant solution. The diluted mixtures (× 0.75) were prepared by taking 150 µL of the mixtures (× 1) and adding 50 µL of the analysis buffer. Final solutions were homogenized by manual agitation before analysis.

Capillary coating. Bare fused silica capillaries of 100 µm i.d. × 58.5 cm total length (50 cm to the detector) were used. Capillaries coatings were performed based on a previously published protocol[38]. HPC was dissolved in water at room temperature to a final concentration of 5% (w/w). The capillaries were flushed 30 min with the polymer solution using the capillary electrophoresis system and then heated in a gas chromatography oven (GC-14 A, Shimadzu, France) under a nitrogen stream of 30 kPa. The temperature program was: 60°C for 10 min, then a 5°C/min gradient from 60°C to 140°C and finally, 140°C for 20 min. Before use and between two samples, the coated capillaries were rinsed 4 min with water and then 4 min with the analysis buffer.

TDA. All experiments were carried out on a 7100 CE Agilent system (Waldbronn, Germany). This system is equipped with a diode array detector (DAD). The temperature of the capillary cartridge was set at 25°C. TDA experiments were performed in triplicates using 12 mbar

mobilization pressure in the frontal mode (continuous injection of the sample in a capillary prefilled with the background electrolyte). The fronts obtained by TDA experiment were derived using Origin software (version 6.0). In case of antigen-adjuvant mixtures analysis, the first derivative of the elution profile was then fitted with two Gaussian functions having the same maximum at a time t_0 corresponding to the maximum of the derived signal, using a home-developed Excel spreadsheet and the Excel solver. The curve fitting was done only on the left part of the first derivative of the elution front, as residual adsorption can distort the right side of the signal. More details about the theoretical background on TDA are given in section 1 of the supporting information.

Transmission electron microscopy (TEM). Solutions of RNase A and SPA09 were prepared at 8 mg/L and 20 mg/L respectively in TRIS buffer (20 mM TRIS, 150 mM NaCl) at pH 7.4. Antigen-adjuvant mixture was prepared by diluting in TRIS buffer a 50/50 (v/v) mixture of RNase A and SPA09 initially at 0.4 g/L and 1 g/L respectively, to a concentration of 8 mg/L and 20 mg/L respectively.

3 µL of the samples were adsorbed onto a carbon continuous coated 300 mesh copper grid (EM Sciences, USA) and incubated for 1 min, the copper grid was previously ionized 90 s with an ELMO ionizer (Cordouan, France). The excess of solutions was removed with filter paper. Then the samples were negatively stained using 2% uranyl acetate. The samples were subsequently air-dried prior to imaging. Electron microscopy data were acquired on a FEI Tecnai G20 (ThermoFisher Scientific, USA) transmission electron microscope operated at 200 kV with a magnification of 50000×. All micrographs were recorded at electron doses between 10 and 15 $e^-/Å^2$ using a Ultrascan 4k x 4k slow-scan CCD camera (Gatan, USA).

Micrographs statistical analysis was performed using ImageJ processing program[39] by using an automatic thresholding and ellipse fitting to determine minimum and maximum ellipse

diameters. The following procedure was used to compare TEM measurements to Taylor diffusion values: (*i*) minor and major ellipse diameter frequency distributions were calculated between 0 and 72 nm with a 2 nm step; (*ii*) the frequency distribution of circular objects was determined as the product of the probability of occurrence of a given diameter for each axis of the ellipse; (*iii*) each frequency was weighted by the total sum of the values; (*iv*) diameter values were transformed in radius.

RESULTS AND DISCUSSION

Development and optimization of TDA for the study of antigen/adjuvant interactions. In a first series of experiments, SPA09 adjuvant, the model proteins and PrSA were analyzed separately. TDA analyses were carried out in frontal mode and the first derivatives were fitted according to equation (S1), (see section S1). Compared to plug mode, frontal mode showed a better sensitivity of detection, a better repeatability of the elution profiles and a better symmetry of the elution profile. An hydrodymanic radius (R_h) of 23 ± 3 nm was determined for SPA09, 1.8 ± 0.1 nm for Cyt C, 2.1 ± 0.1 nm for RNase A and 3.5 ± 0.2 nm for PrSA (see Table 1), according to equations (S-3 and S-4). The results obtained for the model proteins Cyt C and RNase A are consistent with the values found in literature[40,41]. In a second set of experiments, Cyt C-SPA09 interactions were studied by injecting a mixture of 0.8 g/L Cyt C and 1 g/L SPA09 in 20 mM TRIS, 148 mM NaCl, pH 7.4 (thereafter called TRIS buffer). The signal obtained by the first derivative of the elution profile was not symmetrical, as seen in Figure 1A. As the size of the Cyt C / SPA09 complexes was not known, this asymmetrical shape could suggest a partial non-Taylor regime, which can occur for large entities when the analysis time is close or smaller than the characteristic diffusion time in the cross-section of the capillary (i.e. when equation (S6) is not verified)[19]. Thus, different hydrodynamic pressures have been tested to observe the

evolution of the peak shape and symmetry, and different capillary coatings have been also tested to verify that the peak deformation was not due to interactions onto the capillary wall. Figure S2 shows that whatever the hydrodynamic pressure applied, the selected capillary coating (DBWAX, PVA, HPC) or the capillary i.d (50, 75, 100 µm); a deformation of the peak symmetry was observed. These results suggested that the peak deformation was not due to adsorption, nor to convective non-Taylor conditions (i.e. large solutes) since the deformation was still observed for smaller capillary i.d. Lastly, we found that this deformation was due to the difference in composition between the analyzed sample mixture that is continuously introduced in the capillary and the buffer that pre-fill the capillary before injection. As a matter of fact, the addition of SPA09 significantly modifies the viscosity and the ionic strength of the buffer. Moreover, the Cyt C-SPA09 complex is out of equilibrium in the front of the elution profile by dilution effect due to the inherent dispersion during the Taylor analysis. To avoid this effect, and notably to limit the perturbation of the equilibrium, the capillary was first filled with a diluted Cyt C-SPA09 mixture (× 0.75 dilution with the buffer) before injecting the non-diluted (×1) Cyt C-SPA09 mixture, as shown in Figure 1B. The derivative of the second front obtained is symmetrical and can be subsequently used to determine the size of the constituents of the mixture.

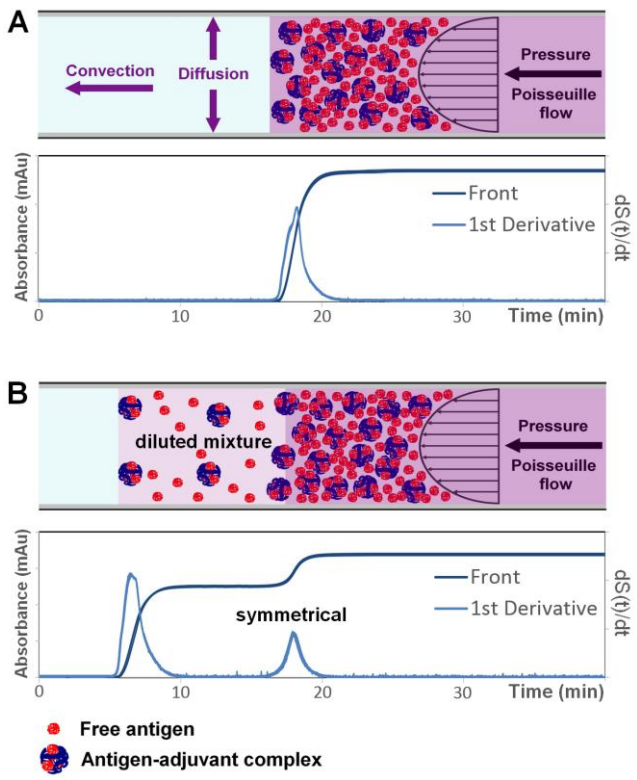

Figure 1: Schematic representation of the Taylor dispersion analysis of antigen-adjuvant mixtures in frontal mode (up) and the corresponding experimental UV traces (down) (triplicate overlays). The capillary is previously filled with the buffer before injection of the concentrated front (×1) (A). A first front of the diluted mixture (×0.75) is injected before the injection of the concentrated antigen-adjuvant mixture (×1) (B). Experimental conditions: HPC-coated capillary of 58.5 cm total length (50 cm to the UV detector) × 100 µm i.d. Buffer: 20 mM TRIS, 148 mM NaCl, pH 7.4. Mobilization pressure: 12 mbar. UV detection: 214 nm. Temperature: 25°C. Concentration in the final mixture (×1): 0.8 g/L Cyt C, 1 g/L SPA09 in the TRIS/NaCl buffer.

Determining the complex size and the free antigen concentration. Two Gaussian curves were required at 214 nm to get a good fitting of the first derivative of the frontal elution profile obtained between (× 0.75) and (× 1) Cyt C-SPA09 mixtures (see Figure 2A and 2B). This bimodal distribution corresponds to the coexistence of Cyt C-SPA09 complex and free Cyt C antigen, as SPA09 does not absorb at 214 nm. The detection of two distinct peaks for each population proves that the kinetics of dissociation of the complex is slow compared to the time scale of the analysis (~15-20 min). Regarding the sizes of the components in the mixture, one of

the two Gaussian peaks led to a hydrodynamic radius of 1.8 ± 0.1 nm, which corresponds to the size of the free Cyt C (see Table 1). The second Gaussian peak led to a size of 12.5 ± 0.2 nm for the Cyt C-SPA09 complex. The fit is only performed on the left side of the Taylorgrams as the right side may be disturbed by adsorption. Fitting the right part of the Taylorgram could lead to overestimated R_h.

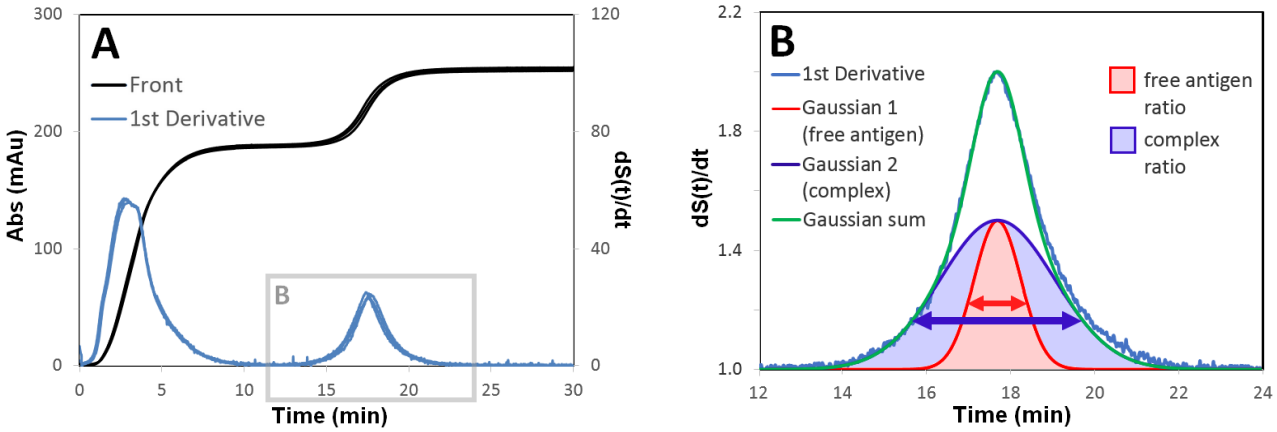

Figure 2: Frontal mode taylorgram and its first derivative (triplicate overlays) obtained for the successive continuous injection of a (×0.75) and (×1) Cyt C-SPA09 mixture (A) and the corresponding zoom (B). Graph (B) shows the fit of the first derivative of the taylorgram with two Gaussian functions according to equation (S2). Experimental conditions as in Figure 1.

It is worth to highlight that the determination of the hydrodynamic radius R_h was obtained using the Stokes−Einstein relation (see equation (S4)), and thus requires the bulk viscosity. This macroscopic viscosity increases of about 1.5 times due to the presence of 1 g/L SPA09 polymer adjuvant in the buffer (η_{TRIS} =0.90 cP; $\eta_{SPA09(\times 0.75)}$ =1.26 cP; $\eta_{SPA09\ (\times 1)}$ =1.37 cP). Therefore, the question arises about which apparent viscosity value should be used for the application of the Stokes-Einstein equation in the case of frontal TDA analysis between (× 0.75) and (× 1) diluted sample mixtures. To answer that question, the size determination of two test molecules (BSA and DMF) was performed in both TRIS buffers with and without SPA09 (see Figure S3). Indeed at pH 7.4, these test molecules do not interact with SPA09 as DMF is a small neutral molecule and BSA is negatively charge (pI = 4.8-5.6[42]) as SPA09. The results demonstrate that the size of BSA

and DMF obtained in TRIS (3.5 nm and 0.25 nm, respectively) are recovered in the presence of SPA09 in the medium with the viscosity value of the diluted mixture (×0.75), i.e. the mixture which is first introduced in the capillary (see Table S1). Taking the viscosity of the (1×) diluted mixture would lead to about 10% lower R_h values than the expected one. Reversely, taking the viscosity of the TRIS buffer would overestimate the R_h value by a factor of +40%.

The same methodology was applied to the RNase A-SPA09 mixture and to the PrSA-SPA09 mixture. Knowing the size of the antigens alone, the temporal variance of one Gaussian was fixed in order to reduce the number of degrees of freedom for the curve fitting. The Peclet number (P_e) and the characteristic time (τ) where calculated to check the validity of the TDA calculations. As detailed in Table 1, the calculations were validated since $\tau > 1.25$ and $P_e > 40$[43,44] (see equations (S5) and (S6)). The hydrodynamic radius of the antigen-adjuvant complexes, the percentage of free antigen in the mixtures and the average number (resp. mass) of antigen bound per adjuvant molecule ($\bar{n}$) (resp. $\bar{m}$), for 0.4 g/L antigen / 1 g/L SPA09 mixtures are reported in Table 1. The average number of bound antigens per adjuvant molecule $\bar{n}$ was calculated using the free antigen concentration [L] at equilibrium in the mixture, according to equation (1):

$$\bar{n} = \frac{[L]_{bound}}{[S]_0} = \frac{[L]_0 - [L]}{[S]_0} = \frac{[L]_0\left(1 - \frac{A_1}{A_1 + A_2}\right)}{[S]_0} \qquad (1)$$

where $[L]_{bound}$ is the molar concentration of the bound antigen, $[S]_0$ is the initial SPA09 molar concentration in the mixture, $[L]_0$ is the initial molar antigen concentration in the mixture, A_1 is the free antigen peak area and A_2 the complexed antigen peak area obtained from the taylorgram fitting (see equation (S2)). At equilibrium, in these mixtures in physiological conditions, an

average number of about $\bar{n}$ =11-13 antigens per adjuvant SPA09 molecule ($\bar{m}$ ~ 3 g antigen per g of SPA09) was determined for RNase A and Cyt C, while 5 PrSA antigens were quantified per SPA09 molecule ($\bar{m}$ ~ 3 g antigen per g of SPA09). The sizes of the complexes were similar for the three antigens (~12 nm). The percentage of free antigen determined was similar for Cyt C and RNase A (~33%) and lower for PrSA (~ 21%).

Table 1: Molar mass (*M*), weight-average hydrodynamic radius (R_h) of the antigens and of the antigen-adjuvant complexes, percentage of free antigen in the mixtures, the average number (resp. mass) of bound antigens per adjuvant molecule ($\bar{n}$) (resp. $\bar{m}$), characteristic time (τ) and Peclet number (P_e) calculated for free antigen and complex, determined from the fitting of the first derivative of the frontal elution profile with two Gaussians (see Figure 2B). Experimental conditions: Buffer: 20 mM TRIS, 148 mM NaCl, pH 7.4 for Cyt C and RNase A. 10 mM PBS, 150 mM NaCl, pH 7.4 for PrSA. Concentrations in the final mixture: 0.4 g/L antigen, 1g/L SPA09. Other experimental conditions as in Figure 1. Experiments were performed in triplicates (error bars = ± one SD).

	Cyt C+SPA09	RNase A+SPA09	PrSA+SPA09
Free antigen *M* (kDa)	12	14	35
Free antigen R_h (nm)	1.8 ± 0.1	2.1 ± 0.1	3.5 ± 0.2
Complex R_h (nm)	12.5 ± 0.2	12.3 ± 0.5	11.8 ± 1.9
% free antigen	32.8 ± 2.3	33.1 ± 0.8	21.4 ± 2.7
$\bar{n}$ (mol/mol)	13.3 ± 0.8	11.3 ± 0.1	5.3 ± 0.2
$\bar{m}$ (g/g)	$(2.7 \pm 0.2) \times 10^{-1}$	$(2.7 \pm 0.1) \times 10^{-1}$	$(3.2 \pm 0.1) \times 10^{-1}$
τ (antigen)	41 ± 1	35 ± 1	20 ± 1
P_e (antigen)	317 ± 2	368 ± 4	610 ± 4
τ (complex)	6 ± 1	6 ± 1	6 ± 1
P_e (complex)	2176 ± 4	2145 ± 8	2045 ± 9

Size comparison between TDA and TEM. Transmission electron microscopy (TEM) was used as an orthogonal method to compare with the results obtained by TDA. Figure 3A-C shows the micrographs obtained by TEM for RNase A, SPA09 and the mixture of the two components. Figure 3D shows the results of the statistical analysis and gives the distribution of the *radii* of the

measured objects. RNase A present a large predominant peak at 2 nm in radius with some larger objects between 4 and 6 nm, which may correspond to groups of dimers-trimers RNAse A molecules. These results are consistent with those observed in TDA, giving an average hydrodynamic radius of 2.1 ± 0.1 nm for RNase A (see Table 1). Three peaks are observed for SPA09 on Figure 3D at 13, 17 and 22 nm. These values, taking into account possible artifacts induced by negative staining approach, can be considered close to the average hydrodynamic radius determined by TDA of 23 ± 3 nm. For the RNase A-SPA09 complexes, a peak ranging from 7 to 16 nm with a maximum centered on 12 nm is observed on Figure 3D. These results are in agreement with TDA, giving an average hydrodynamic radius of 12.3 ± 0.5 nm for the same RNase A/SPA09 ratio. In addition to these major forms, large micrometric aggregates in small numbers have been observed by TEM. Overall, the results obtained by the two orthogonal methods are consistent and TEM confirmed that the *radii* of RNase A-SPA09 complexes tend to be smaller than the radius of SPA09 alone, as observed for polyplexe formation[21]. The TEM data obtained should however be taken with caution as structural artifacts due to staining, dehydration and imaging under a non-native environment may affect particle size distribution. TEM methodology remains useful and continues to be widely used[45,46].

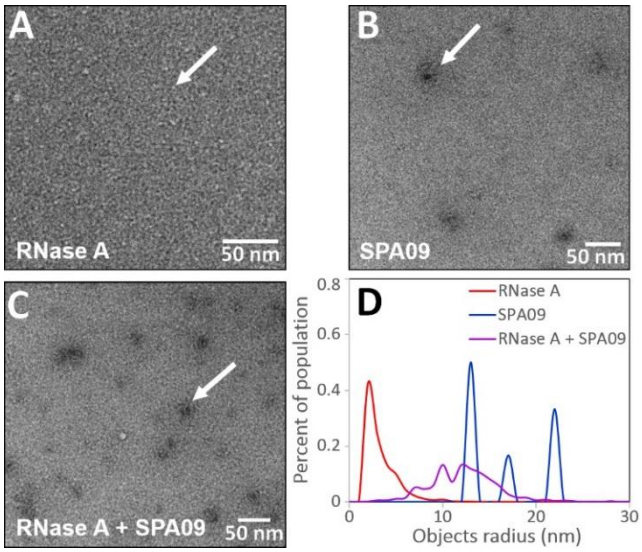

Figure 3: TEM micrographs of RNase A (A), SPA09 (B) and RNase A-SPA09 mixture (C). Chart (D) shows the *radii* distribution of automatic selected objects. Experimental conditions: Samples were prepared in TRIS buffer (20 mM TRIS, 150 mM NaCl) at pH 7.4. RNase A concentration alone (A) and in the mixture (C) is 8 mg/L. SPA09 concentration alone (B) and in the mixture (C) is 20 mg/L. Samples were stained with uranyl acetate. TEM was operated at 200 kV, magnification of 50000×, electron doses between 10 and 15 e−/Å^2. Arrows point to a selected object example.

Adsorption isotherms. The access to the percentage of free antigen owing to TDA methodology allows to calculate the average number of bound antigens per adjuvant for different introduced antigen/adjuvant ratios and to plot the adsorption isotherm of the antigens onto the adjuvant. The adsorption isotherm is the graphical representation of the average number of bound antigens per adjuvant $\bar{n}$ as a function of the free antigen concentration $[L]$. Adsorption isotherms of the two model proteins (Cyt C and RNase A) and the vaccine antigen PrSA on SPA09 were plotted in the basis of triplicates analysis on different antigen/adjuvant ratios (see Figure 4A). The raw data (taylorgrams) are displayed in Figure S4. BSA-SPA09 mixtures were also analyzed as a control for the absence of interaction. As expected, 100% of free BSA has been detected in the mixture (single Gaussian curve fitting due to the absence of interaction). For the other antigens, all the taylorgrams were fitted with two Gaussian curves according to equation (S2).

Langmuir adsorption model was used to fit the obtained isotherm. In Langmuir model, it is assumed that the substrate (or adjuvant, *S*) contains *n* independent interaction sites of equal energy and the occupation of one site does not influence the occupation of the other. In the framework of this model, the adsorption isotherm is described by equation (2):

$$\bar{n} = \frac{nk[L]}{1+k[L]} \qquad (2)$$

where *k* is the intrinsic binding site constant and *n* the maximum number of interacting sites. *n* and *k* can be obtained by nonlinear curve fitting of the experimental isotherm (see dotted lines in Figure 4A).

When the entire isotherm can be obtained experimentally, the best way to get the interaction parameters is a nonlinear curve fitting. The maximum number of interacting sites *n* corresponds to the value of $\bar{n}$ at saturation of the isotherm. It can be observed on Figure 4A that the three adsorption isotherms obtained do not display any saturation plateau on the concentration range studied. It is worth noting that it was not possible to further increase the antigen concentration, and thus reach the saturation plateau, due to solubility issues. Thus, the *n* value could not be directly obtained from the isotherm plateau. However, the slope at the origin of the isotherm can give access to the first successive binding constant $K_1 = n \times k$ as demonstrated by the first derivative of equation (3):

$$\lim_{[L]\to 0} \frac{d\bar{n}}{d[L]} = \lim_{[L]\to 0} \frac{nk}{(1+k[L])^2} = nk \qquad (3)$$

The experimental determination of $K_1 = n \times k$ allows a first ranking of the interactions: $K_{1PrSA} > K_{1\text{Cyt C}} \approx K_{1\text{RNase A}}$, (see Table 2). It should be noted that K_1 represents the equilibrium constant

between a free substrate (or adjuvant) and a substrate interacting with only one antigen (whatever the position of the antigen on the adjuvant). It should not be confused with *k* the intrinsic binding site constant, which is the equilibrium constant associated to one interacting site (free *vs* occupied interacting site). An estimation of the *k* value, can be derived from the slope of the Scatchard representation which consists in plotting $\frac{\bar{n}}{[L]}$ as a function of $\bar{n}$ according to equation (4):

$$\frac{\bar{n}}{[L]} = nk - k\bar{n} \qquad (4)$$

The Scatchard representation obtained for the Cyt C-SPA09, RNase A-SPA09 and PrSA-SPA09 mixtures are presented in Figure 4B. The obtained *k* values varied between 5.2× 10^3 and 8.8× 10^4 M^{-1} and ranked as followed: $k_{PrSA} > k_{\text{RNase A}} > k_{\text{Cyt C}}$. Knowing K_1 and *k*, allows to estimate the total number of interaction sites (*n*) which varied between 27 for PrSA and 250 for Cyt C. By replacing *n* and *k* in the expression of the Langmuir model equation (1), the fits of the isotherms were represented by the dotted lines in Figure 4A, showing good agreement with the

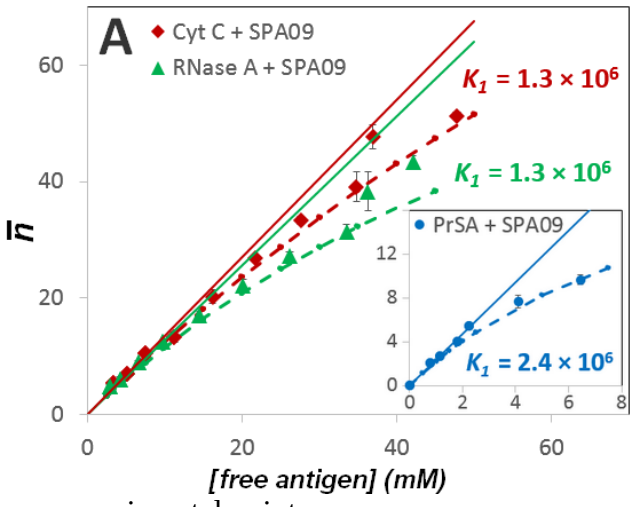

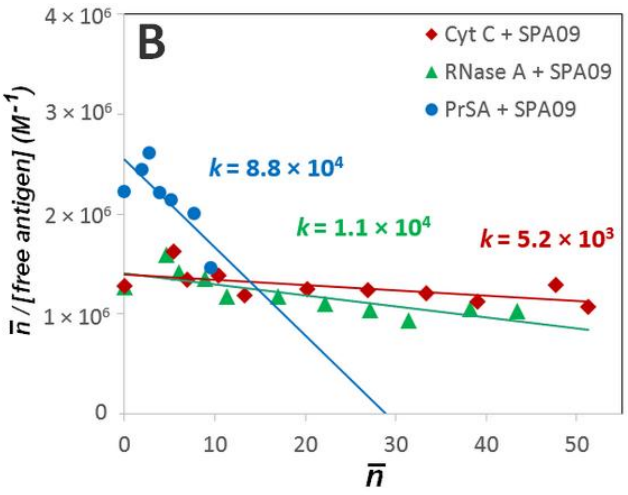

experimental points.

Figure 4: Isotherms of adsorption obtained by TDA for the interaction between Cyt C, RNase A and PrSA and SPA09 adjuvant (A) and the corresponding Scatchard plots (B). The first successive interaction constant $K_1=nk$ is determined from the slope at the origin of the isotherm in Figure 4A. The intrinsic binding site constant k was obtained from the slopes of the Scatchard representation in Figure 4B. Fitting curves (dotted lines represented in Figure 4A) were plotted with the k and n values using Langmuir model of independent sites of equal energy (equation (9)). Introduced concentrations in the mixtures: 1g/L SPA09, Cyt C and RNase A: 0.15; 0.20; 0.30; 0.40; 0.60; 0.80; 1.00; 1.20; 1.40 and 1.60 g/L, PrSA: 0.15; 0.20; 0.35; 0.40; 0.50; 0.60; 0.70 and 0.80 g/L. Other experimental conditions as in Figure 1.

TDA / FACCE comparison. The interactions between Cyt C, RNase A, PrSA and SPA09 have already been studied in a previous work by frontal analysis continuous capillary electrophoresis (FACCE)[22]. The binding parameters determined by TDA in this work are compared with those previously obtained by FACCE in Table 2. The percentage of free antigen, the average number of bound antigen per adjuvant molecule $\bar{n}$ and the average mass of bound antigen per g of adjuvant $\bar{m}$ for a 0.4 g/L antigen + 1g/L SPA09 mixture, and the first successive interaction constant K_1 measured by TDA and FACCE were in very good agreement. The values obtained for the intrinsic binding site constant k and the stoichiometry at saturation (expressed in number (n) or in mass (m)) obtained by TDA and FACCE were also comparable even if larger discrepancies could be observed for the n (or m) values, notably for Cyt. C, due to the uncertainty of the determination by extrapolation / linearization. These values nevertheless remained of the same order of magnitude between the two methods.

The analyses carried out allows to highlight the advantages and disadvantages of each methodology. One advantage of the FACCE methodology is that it gives direct access to the concentration of free antigen by the measurement of the height of the front. Data analysis is therefore easier and faster. Moreover, in the case of the FACCE it is not necessary to pre-fill the capillary with a diluted fraction (0.75×) of the mixture and thus the sensitivity of detection is better in FACCE. On the other side, TDA gives not only access to the binding parameters ($\bar{n}$, n,

k) but also to the constituents' size (including the complex size), which is not accessible by FACCE. TDA is also more straightforward and more robust, since there is no electric field to apply, no possible electroosmotic flow fluctuations and no redox reactions at the electrodes (i.e. no pH alteration of the analysis sample). In addition, TDA is an absolute method which does not require calibration (neither for the size determination, nor for the ligand free proportion).

Table 2: Comparison of the percentage of free antigen, the average number (resp. mass) of bound antigens per adjuvant molecule ($\bar{n}$, resp. $\bar{m}$), the first successive interaction constant K_1, the intrinsic binding site constant k and the stoichiometry of the interaction at saturation expressed in number of interaction sites (n) and in mass ratio (m) obtained by TDA and by FACCE using Langmuir model of independent sites of equal energy. [a] Concentration in the final mixture: 0.4 g/L antigen, 1g/L SPA09. [b] 20 mM TRIS, 148 mM NaCl, pH 7.4[c]. 10 mM PBS, 150 mM NaCl, pH 7.2.

	Cyt C+SPA09		RNase A+SPA09		PrSA+SPA09	
	FACCE [b]	TDA [b]	FACCE [b]	TDA [b]	FACCE [b]	TDA [c]
% *free antigen* [a]	33.9 ± 1.0	32.8 ± 4.3	38.1 ± 1.4	33.1 ± 0.8	29.2 ± 0.7	21.4 ± 2.7
$\bar{n}$ (mol/mol) [a]	13.0 ± 0.2	13.3 ± 0.8	10.4 ± 0.2	11.3 ± 0.1	4.9 ± 0.1	5.3 ± 0.2
$\bar{m}$ (g/g) [a]	(2.6 ± 0.1) × 10^{-1}	(2.7 ± 0.2) × 10^{-1}	(2.5 ± 0.1) × 10^{-1}	(2.7 ± 0.1) × 10^{-1}	(2.9 ± 0.1) × 10^{-1}	(3.2 ± 0.1) × 10^{-1}
$K_1 = nk$ (M^{-1})	(1.2 ± 0.1) × 10^6	(1.3 ± 0.1) × 10^6	(1.1 ± 0.1) × 10^6	(1.3 ± 0.1) × 10^6	(1.5 ± 0.1) × 10^6	(2.4 ± 0.1) × 10^6
k (M^{-1})	(8.4 ± 2.1) × 10^3	(5.2 ± 2.2) × 10^3	(1.3 ± 0.1) × 10^4	(1.1 ± 0.3) × 10^4	(5.2 ± 2.0) × 10^4	(8.8 ± 2.9) × 10^4
n (mol/mol)	149 ± 51	250 ± 125	86 ± 12	116 ± 42	28 ± 12	27 ± 10
m (g/g)	3.0 ± 1.0	5.1 ± 2.6	2.0 ± 0.3	2.7 ± 1.0	1.7 ± 0.7	1.6 ± 0.6

CONCLUSIONS

The aim of this work was to develop a new methodology to characterize the interactions between vaccine antigens and adjuvants. TDA method was found to be an excellent way to simultaneously determine the size of the antigen-adjuvant complexes, and the percentage of free antigen in the mixture, under physiological conditions. The determination of percentage of free antigen allowed to plot the adsorption isotherms and determine the binding constants and stoichiometry of the interaction using Langmuir model of independent sites of equal energy. The average hydrodynamic radius of the antigen-adjuvant complexes obtained by TDA were confirmed by TEM measurements (both ~12 nm). The binding parameters (*k* and *n*) were compared to those obtained in a previous study by FACCE and were in relatively good agreement. The same methodology could be used with fluorescently labeled antigens to study lower concentrations and stronger binding constant. Due to its simplicity, the absence of size calibration, the low sample consumption and the high degree of automation, TDA has the potential to be a method of reference to characterize antigen-adjuvant interactions in future vaccines.

ACKNOWLEDGMENTS

This work was partly funded by Sanofi Pasteur under a Cooperative Research and Development Agreement with the University of Montpellier and the CNRS.

SUPPORTING INFORMATION

Theoretical background on TDA. Fit of the first derivative of the elution front obtained for Cyt C, RNase A, PrSA and SPA09 analyzed separately. Influence of different neutral coatings (and/or

capillary i.d.) and different hydrodynamic mobilizing pressures on taylorgrams of Cyt C-SPA09 mixture. Taylorgrams of BSA and DMF in TRIS buffer alone and in presence of SPA09 to study the impact of viscosity. Viscosity impact on the determination of the weight-average hydrodynamic radius (Rh in nm) of two solutes (BSA and DMF). Taylorgrams obtained in triplicates for the isotherm of adsorption.

REFERENCES

(1) Veve, M. P.; Athans, V. Vaccines - Chapter 30. In *Side Effects of Drugs Annual*; Ray, S. D., Ed.; Elsevier, **2019**; Vol. 41, pp 351–372. https://doi.org/10.1016/bs.seda.2019.07.016.

(2) Rappuoli, R.; Pizza, M.; Del Giudice, G.; De Gregorio, E. Vaccines, New Opportunities for a New Society. *Proc. Natl. Acad. Sci.* **2014**, *111* (34), 12288–12293. https://doi.org/10.1073/pnas.1402981111.

(3) Burke, E. E.; Kodumudi, K.; Ramamoorthi, G.; Czerniecki, B. J. Vaccine Therapies for Breast Cancer. *Surg. Oncol. Clin. N. Am.* **2019**, *28* (3), 353–367. https://doi.org/10.1016/j.soc.2019.02.004.

(4) Marciani, D. J. New Th2 Adjuvants for Preventive and Active Immunotherapy of Neurodegenerative Proteinopathies. *Drug Discov. Today* **2014**, *19* (7), 912–920. https://doi.org/10.1016/j.drudis.2014.02.015.

(5) Reed, S. G.; Orr, M. T.; Fox, C. B. Key Roles of Adjuvants in Modern Vaccines. *Nat. Med.* **2013**, *19* (12), 1597–1608. https://doi.org/10.1038/nm.3409.

(6) HogenEsch, H.; O'Hagan, D. T.; Fox, C. B. Optimizing the Utilization of Aluminum Adjuvants in Vaccines: You Might Just Get What You Want. *Npj Vaccines* **2018**, *3* (1), 1–11. https://doi.org/10.1038/s41541-018-0089-x.

(7) Garçon, N.; Friede, M. Evolution of Adjuvants Across the Centuries - Chapter 6. In *Plotkin's Vaccines*; **2018**; pp 61–74.

(8) Schijns, V. E. J. C. Vaccine Adjuvants' Mode of Action: Unraveling ''the Immunologist's Dirty Little Secret" - Chapter 1. In *Immunopotentiators in Modern Vaccines*; O'Hagan, D. T., Ed.; Academic Press, **2017**; pp 1–22. https://doi.org/10.1016/B978-0-12-804019-5.00001-3.

(9) Yan, S.; Gu, W.; Xu, Z. P. Re-Considering How Particle Size and Other Properties of Antigen–Adjuvant Complexes Impact on the Immune Responses. *J. Colloid Interface Sci.* **2013**, *395*, 1–10. https://doi.org/10.1016/j.jcis.2012.11.061.

(10) Oyewumi, M. O.; Kumar, A.; Cui, Z. Nano-Microparticles as Immune Adjuvants: Correlating Particle Sizes and the Resultant Immune Responses. *Expert Rev. Vaccines* **2010**, *9* (9), 1095–1107. https://doi.org/10.1586/erv.10.89.

(11) Pedersen, M. E.; Gad, S. I.; Østergaard, J.; Jensen, H. Protein Characterization in 3D: Size, Folding, and Functional Assessment in a Unified Approach. *Anal. Chem.* **2019**, *91* (8), 4975–4979. https://doi.org/10.1021/acs.analchem.9b00537.

(12) Leclercq, L.; Saetear, P.; Rolland-Sabaté, A.; Biron, J.-P.; Chamieh, J.; Cipelletti, L.; Bornhop, D. J.; Cottet, H. Size-Based Characterization of Polysaccharides by Taylor Dispersion Analysis with Photochemical Oxidation or Backscattering Interferometry Detections. *Macromolecules* **2019**, *52* (12), 4421–4431. https://doi.org/10.1021/acs.macromol.9b00605.

(13) Urban, D. A.; Milosevic, A. M.; Bossert, D.; Crippa, F.; Moore, T. L.; Geers, C.; Balog, S.; Rothen-Rutishauser, B.; Petri-Fink, A. Taylor Dispersion of Inorganic Nanoparticles and Comparison to Dynamic Light Scattering and Transmission Electron Microscopy. *Colloid Interface Sci. Commun.* **2018**, *22*, 29–33. https://doi.org/10.1016/j.colcom.2017.12.001.
(14) Chamieh, J.; Biron, J. P.; Cipelletti, L.; Cottet, H. Monitoring Biopolymer Degradation by Taylor Dispersion Analysis. *Biomacromolecules* **2015**, *16* (12), 3945–3951. https://doi.org/10.1021/acs.biomac.5b01260.
(15) Ibrahim, A.; Meyrueix, R.; Pouliquen, G.; Chan, Y. P.; Cottet, H. Size and Charge Characterization of Polymeric Drug Delivery Systems by Taylor Dispersion Analysis and Capillary Electrophoresis. *Anal. Bioanal. Chem.* **2013**, *405* (16), 5369–5379. https://doi.org/10.1007/s00216-013-6972-4.
(16) Liu, T.; Oukacine, F.; Collet, H.; Commeyras, A.; Vial, L.; Cottet, H. Monitoring Surface Functionalization of Dendrigraft Poly-l-Lysines via Click Chemistry by Capillary Electrophoresis and Taylor Dispersion Analysis. *J. Chromatogr. A* **2013**, *1273*, 111–116. https://doi.org/10.1016/j.chroma.2012.11.074.
(17) Hulse, W.; Forbes, R. A Taylor Dispersion Analysis Method for the Sizing of Therapeutic Proteins and Their Aggregates Using Nanolitre Sample Quantities. *Int. J. Pharm.* **2011**, *416* (1), 394–397. https://doi.org/10.1016/j.ijpharm.2011.06.045.
(18) Chamieh, J.; Cottet, H. Size-Based Characterisation of Nanomaterials by Taylor Dispersion Analysis - Chapter 9. In *Colloid and Interface Science in Pharmaceutical Research and Development*; Ohshima, H., Makino, K., Eds.; Elsevier, **2014**; pp 173–192. https://doi.org/10.1016/B978-0-444-62614-1.00009-0.
(19) Chamieh, J.; Leclercq, L.; Martin, M.; Slaoui, S.; Jensen, H.; Østergaard, J.; Cottet, H. Limits in Size of Taylor Dispersion Analysis: Representation of the Different Hydrodynamic Regimes and Application to the Size-Characterization of Cubosomes. *Anal. Chem.* **2017**, *89* (24), 13487–13493. https://doi.org/10.1021/acs.analchem.7b03806.
(20) Cottet, H.; Biron, J.-P.; Cipelletti, L.; Matmour, R.; Martin, M. Determination of Individual Diffusion Coefficients in Evolving Binary Mixtures by Taylor Dispersion Analysis: Application to the Monitoring of Polymer Reaction. *Anal. Chem.* **2010**, *82* (5), 1793–1802. https://doi.org/10.1021/ac902397x.
(21) Leclercq, L.; Reinhard, S.; Chamieh, J.; Döblinger, M.; Wagner, E.; Cottet, H. Fast Characterization of Polyplexes by Taylor Dispersion Analysis. *Macromolecules* **2015**, *48* (19), 7216–7221. https://doi.org/10.1021/acs.macromol.5b01824.
(22) Malburet, C.; Leclercq, L.; Cotte, J.-F.; Thiebaud, J.; Cottet, H. Study of Interactions between Antigens and Polymeric Adjuvants in Vaccines by Frontal Analysis Continuous Capillary Electrophoresis. *Biomacromolecules* **2020**, *21* (8), 3364–3373. https://doi.org/10.1021/acs.biomac.0c00782.
(23) Høgstedt, U. B.; Schwach, G.; van de Weert, M.; Østergaard, J. Taylor Dispersion Analysis as a Promising Tool for Assessment of Peptide-Peptide Interactions. *Eur. J. Pharm. Sci.* **2016**, *93*, 21–28. https://doi.org/10.1016/j.ejps.2016.07.015.
(24) Quinn, J. G. Evaluation of Taylor Dispersion Injections: Determining Kinetic/Affinity Interaction Constants and Diffusion Coefficients in Label-Free Biosensing. *Anal. Biochem.* **2012**, *421* (2), 401–410. https://doi.org/10.1016/j.ab.2011.11.023.
(25) Jensen, H.; Østergaard, J. Flow Induced Dispersion Analysis Quantifies Noncovalent Interactions in Nanoliter Samples. *J. Am. Chem. Soc.* **2010**, *132* (12), 4070–4071. https://doi.org/10.1021/ja100484d.
(26) Bielejewska, A.; Bylina, A.; Duszczyk, K.; Fiałkowski, M.; Hołyst, R. Evaluation of Ligand-Selector Interaction from Effective Diffusion Coefficient. *Anal. Chem.* **2010**, *82* (13), 5463–5469. https://doi.org/10.1021/ac1008207.

(27) Jensen, H.; Larsen, S. W.; Larsen, C.; Østergaard, J. Physicochemical Profiling of Drug Candidates Using Capillary-Based Techniques. *J. Drug Deliv. Sci. Technol.* **2013**, *23* (4), 333–345. https://doi.org/10.1016/S1773-2247(13)50050-5.
(28) Diamantstein, T., Wagner, B., Beyse, I., Odenwald, M.V., Schultz, G. Stimulation of Humoral Antibody Formation by Polyanions. The Effect of Polyacrylic Acid on the Primary Immune Response in Mice Immunized with Sheep Red Blood Cells. *Eur. J. Immunol.* **1971**, 335–340. https://doi.org/10.1002/eji.1830010506.
(29) Mumford, J. A.; Wilson, H.; Hannant, D.; Jessett, D. M. Antigenicity and Immunogenicity of Equine Influenza Vaccines Containing a Carbomer Adjuvant. *Epidemiol. Infect.* **1994**, *112* (02), 421–437. https://doi.org/10.1017/S0950268800057848.
(30) Mair, K. H.; Koinig, H.; Gerner, W.; Höhne, A.; Bretthauer, J.; Kroll, J. J.; Roof, M. B.; Saalmüller, A.; Stadler, K.; Libanova, R. Carbopol Improves the Early Cellular Immune Responses Induced by the Modified-Life Vaccine Ingelvac PRRS® MLV. *Vet. Microbiol.* **2015**, *176* (3), 352–357. https://doi.org/10.1016/j.vetmic.2015.02.001.
(31) Cotte, J.-F.; Bouadam, A.; Sordoillet, A.; Jaudinaud, I.; Chambon, V.; Talaga, P. Determination of Molecular Size Parameters and Quantification of Polyacrylic Acid by High Performance Size-Exclusion Chromatography with Triple Detection. *Anal. Bioanal. Chem.* **2017**, *409* (8), 2083–2092. https://doi.org/10.1007/s00216-016-0155-z.
(32) Krashias, G.; Simon, A.-K.; Wegmann, F.; Kok, W.-L.; Ho, L.-P.; Stevens, D.; Skehel, J.; Heeney, J. L.; Moghaddam, A. E.; Sattentau, Q. J. Potent Adaptive Immune Responses Induced against HIV-1 Gp140 and Influenza Virus HA by a Polyanionic Carbomer. *Vaccine* **2010**, *28* (13), 2482–2489. https://doi.org/10.1016/j.vaccine.2010.01.046.
(33) Rigaut, G.; Parisot, A.; De Luca, K.; Andreoni, C.; Remolue, L.; Garinot, M.; Cotte, J.-F.; Probeck-Quellect, P.; Haensler, J.; Chambon, V.; Talaga, P. Novel Immunogenic Formulations Comprising Linear or Branched Polyacrylic Acid Polymer Adjuvants. Patent WO/2017/218819 2017.
(34) Bommier, E.; Chapat, L.; Guiot, A. L.; Hilaire, F.; Cariou, C.; Poulet, H.; Pialot, D.; De Luca, K. Multivariate Analysis of the Immune Response to Different Rabies Vaccines. *Vet. Immunol. Immunopathol.* **2020**, *220*, 1–6. https://doi.org/10.1016/j.vetimm.2019.109986.
(35) Daum, R. S. Staphylococcus Aureus Vaccines. In *Vaccines (Sixth Edition)*; Plotkin, S. A., Orenstein, W. A., Offit, P. A., Eds.; 2013; pp 1161–1168. https://doi.org/10.1016/B978-1-4557-0090-5.00060-4.
(36) Hajighahramani, N.; Eslami, M.; Negahdaripour, M.; Ghoshoon, M. B.; Dehshahri, A.; Erfani, N.; Heidari, R.; Gholami, A.; Nezafat, N.; Ghasemi, Y. Computational Design of a Chimeric Epitope-Based Vaccine to Protect against Staphylococcus Aureus Infections. *Mol. Cell. Probes* **2019**, *46*, 101414. https://doi.org/10.1016/j.mcp.2019.06.004.
(37) O'Brien, E. C.; McLoughlin, R. M. Considering the 'Alternatives' for Next-Generation Anti-Staphylococcus Aureus Vaccine Development. *Trends Mol. Med.* **2019**, *25* (3), 171–184. https://doi.org/10.1016/j.molmed.2018.12.010.
(38) Shen, Y.; Smith, R. D. High-Resolution Capillary Isoelectric Focusing of Proteins Using Highly Hydrophilic-Substituted Cellulose-Coated Capillaries. *J. Microcolumn Sep.* **2000**, *12* (3), 135–141. https://doi.org/10.1002/(SICI)1520-667X(2000)12:3<135::AID-MCS2>3.0.CO;2-5.
(39) Abramoff, M. D.; Magelhaes, P. J.; Ram, S. J. Image Processing with ImageJ. *Biophotonics Int.* **2004**, *volume 11* (issue 7), 36–42.
(40) Ghosh, C.; Asif Amin, M. D.; Jana, B.; Bhattacharyya, K. Size and Structure of Cytochrome-c Bound to Gold Nano-Clusters: Effect of Ethanol. *J. Chem. Sci.* **2017**, *129* (7), 841–847. https://doi.org/10.1007/s12039-017-1239-9.

(41) Nöppert, A.; Gast, K.; Müller-Frohne, M.; Zirwer, D.; Damaschun, G. Reduced-Denatured Ribonuclease A Is Not in a Compact State. *FEBS Lett.* **1996**, *380* (1–2), 179–182. https://doi.org/10.1016/0014-5793(96)00048-8.
(42) Barbosa, L. R. S.; Ortore, M. G.; Spinozzi, F.; Mariani, P.; Bernstorff, S.; Itri, R. The Importance of Protein-Protein Interactions on the PH-Induced Conformational Changes of Bovine Serum Albumin: A Small-Angle X-Ray Scattering Study. *Biophys. J.* **2010**, *98* (1), 147–157. https://doi.org/10.1016/j.bpj.2009.09.056.
(43) Bello, M. S.; Rezzonico, R.; Righetti, P. G. Use of Taylor-Aris Dispersion for Measurement of a Solute Diffusion Coefficient in Thin Capillaries. *Science* **1994**, *266* (5186), 773–776. https://doi.org/10.1126/science.266.5186.773.
(44) Cottet, H.; Biron, J.-P.; Martin, M. On the Optimization of Operating Conditions for Taylor Dispersion Analysis of Mixtures. *Analyst* **2014**, *139* (14), 3552–3562. https://doi.org/10.1039/C4AN00192C.
(45) De Carlo, S.; Harris, J. R. Negative Staining and Cryo-Negative Staining of Macromolecules and Viruses for TEM. *Micron* **2011**, *42* (2), 117–131. https://doi.org/10.1016/j.micron.2010.06.003.
(46) Harris, J. R.; Roos, C.; Djalali, R.; Rheingans, O.; Maskos, M.; Schmidt, M. Application of the Negative Staining Technique to Both Aqueous and Organic Solvent Solutions of Polymer Particles. *Micron* **1999**, *30* (4), 289–298. https://doi.org/10.1016/S0968-4328(99)00034-7.

For Table of Contents use only: